2010 IEEE/ASME International Conference on
Advanced Intelligent Mechatronics
Montréal, Canada, July 6-9, 2010

On the Use of Free-floating Space Robots in the Presence of Angular Momentum

Kostas Nanos and Evangelos Papadopoulos, *Senior Member, IEEE*

***Abstract*— Free–floating space manipulator systems, have their thrusters turned off and exhibit nonholonomic behavior due to angular momentum conservation. Here, the initial system angular momentum is not assumed to be zero and therefore the manipulator end effector cannot remain in a position for indefinite time. The system kinematics and dynamics constraints are studied yielding a subset of a system's reachable workspace where the end effector can remain indefinitely. The application of the methodology is illustrated using an example. To demonstrate the concept, an experimental space robot simulator was developed and its mechatronics aspects are presented briefly.**

I. Introduction

Robotic manipulators are already playing an important role in planetary exploration and in tasks on orbit because of their ability to act in environments that are inaccessible or too risky for humans. On orbit robotic systems, or free–flying space manipulator systems, include a thruster-equipped satellite base with robotic manipulators mounted on it. An early example of such a system is the ETS–7 [1]. During manipulation or capture operations [2], it is desired to have the base thrusters turned off to avoid interactions with the target. In this case, the system operates in a free–floating mode. In this mode, dynamic coupling exists between the manipulator and the base, and therefore manipulator motions induce disturbances to the system's base. Since the thrusters are off, the spacecraft is permitted to translate and rotate in response to manipulator motions. This mode of operation is feasible only when no external forces and torques act on the system and when the initial momentum of the system is zero. However, during operations, small amounts of angular momentum tend to accumulate. In general, this momentum can be handled for a short period of time. If it increases above a limit, thruster jets must be turned on to reduce it. However, their extensive use limits a robotic system's useful life span. Therefore, the ability to work on orbit under the presence of small amounts of angular momentum is important and is studied here.

A free-floating space robot with initial angular momentum is an affine system with a drift term. This term is due to the angular momentum and complicates the path planning and control of such systems. To date, a limited number of studies have dealt with such systems. Matsuno and Saito have proposed an attitude point-to-point control law, considering a planar two–link space robot with initial angular momentum, i.e. a typical example of a 3–state and 2–input affine system with a drift term, [3]. Although the controller takes the system to the desired location, the system drifts away due to the non-zero angular momentum.

Test facilities simulating a space-like environment have been developed in the USA, Europe and Japan. The MIT's SPHERES project consists of three small satellites, each attached to a puck that hovers over a glass table using air-bearings, and moves using thrusters [4]. Stanford University's Aerospace Robotics Laboratory also has built a planar simulator, where three active free-flying vehicles and one passive target vehicle hover over a granite table using air-bearings. The active vehicles are propelled by thrusters [5]. The University of Padova has developed a robot with an anthropomorphic manipulator that hovers over a small table using air-bearings, and moves using thrusters [6]. At Tokyo Institute of Technology, the simulator consists of a 6-DOF manipulator hovering over a flat floor using air-bearings [7].

In this paper, we study the effect of initial angular momentum on a free-floating space robot, see Fig. 1. We examine if workspace locations exist in which it is possible to have the system's end-effector fixed, in the presence of non-zero angular momentum. This is important when the manipulator is engaged in a monitoring or maintenance task. In general, in the presence of angular momentum, the manipulator end effector cannot remain in a position for an indefinite time. The proposed method exploits the kinematics and dynamics constraints, which arise from the system's dynamics, and allows the computation of such locations for a given system. The method is illustrated by an example. A successful deployment requires experimental task validation. With this aim, we present the main characteristics of the experimental space robot simulator developed at the National Technical University of Athens (NTUA), focusing at its mechatronics characteristics.

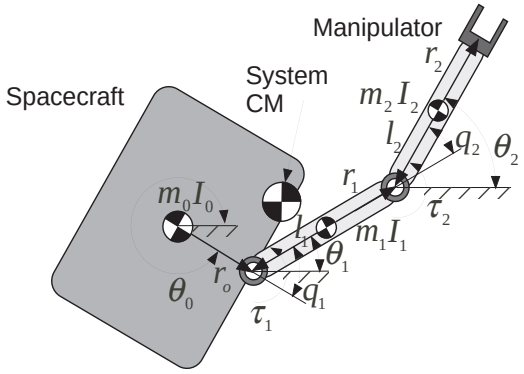

Fig. 1. A Free-floating Space Manipulator System consisting of a base and a manipulator.

Kostas Nanos and Evangelos Papadopoulos are with the Department of Mechanical Engineering, National Technical University of Athens (NTUA), Greece (phone: +30-210-772-2643, 1440; fax: +30-210-772-1450; e-mail: egpapado@central.ntua.gr, knanos@mail.ntua.gr).

II. Dynamics of Free-Floating Space Manipulators

A space manipulator system consists of a spacecraft and a manipulator mounted on it, see Fig. 1. When the system is operating in free-floating mode, the spacecraft's attitude control system is turned off. In this mode, no external forces and torques act on the system, and hence the spacecraft translates and rotates in response to manipulator motions.

This section develops briefly the equations of motion of a rigid free-floating system when the angular momentum is not zero. This can occur due to small collisions with the environment or due to the inaccurate on-off attitude controller. For simplicity, the manipulator is assumed to have revolute joints and an open chain kinematic configuration, so that, in a system with N degree-of-freedom (dof) manipulator, there will be $N+6$ dof.

Under the assumptions of absence of external forces, the system Center of Mass (CM) does not accelerate, and the system linear momentum, is constant. With the further assumption of zero initial linear momentum, the system CM remains fixed in inertial space, and the origin, O, can be chosen to be the system's CM. For simplicity, we focus on a planar free-floating robotic system consisting of a two degree-of-freedom (dof) manipulator mounted on a spacecraft base, see Fig. 1. This system is also appropriate for the space robotics emulator described later in this paper. For this system, the conservation of angular momentum can be written as

$$D_0\,\dot\theta_0 + D_1\,\dot\theta_1 + D_2\,\dot\theta_2 = h_0 \tag{1}$$

where θ_0 is the spacecraft attitude, θ_1, θ_2 are the manipulator absolute angles, see Fig. 1, and h_0 is the initial angular momentum about the system CM, [8]. The coefficients D_0, D_1 and D_2 depend on system parameters, are functions of the manipulator joint angles $\mathbf{q}=\left[q_1,\, q_2\right]^T$ and are given in Appendix A.

The end effector position is given by [8]:

$$x_E = \alpha\, c_{\theta_0} + \beta\, c_{\theta_1} + \gamma\, c_{\theta_2} \tag{2a}$$

$$y_E = \alpha\, s_{\theta_0} + \beta\, s_{\theta_1} + \gamma\, s_{\theta_2} \tag{2b}$$

where α,β,γ are constant terms, functions of the system mass properties, see Appendix A, and $c_{\theta_i}=\cos\theta_i$, $s_{\theta_i}=\sin\theta_i$, $i=0,1,2$. The end effector linear velocity can be found by differentiating (2).

The system kinetic energy is given by

$$T = \frac{1}{2}\sum_{i=0}^{2} m_i\, \mathbf{v}_i^T\, \mathbf{v}_i + \frac{1}{2}\sum_{i=0}^{2} I_i\,\omega_i^2 \tag{3}$$

where $\mathbf{v}_i$ is the linear velocity of the CM of body i expressed in the spacecraft frame and given by,

$$\mathbf{v}_i = \mathbf{F}_{1i}(\mathbf{q})[\dot\theta_0,\, \dot{\mathbf{q}}^T]^T,\ i=0,\,1,\,2 \tag{4}$$

and ω_i and I_i are the angular velocity and the polar inertia of body i. The spacecraft angular velocity is $\omega_0=\dot\theta_0$ and the angular velocities of the other bodies, expressed in the spacecraft frame are given by,

$$\omega_i = \mathbf{F}_{2i}(\mathbf{q})[\dot\theta_0,\, \dot{\mathbf{q}}^T]^T,\ i=1,\,2 \tag{5}$$

In Eqs. (4) – (5) $\mathbf{F}_{1i}(\mathbf{q})$, $\mathbf{F}_{2i}(\mathbf{q})$ are matrices of appropriate dimensions. The potential energy due to gravity is zero and since the system is assumed to be rigid, the potential energy due to flexibility is also zero. Then, the system Lagrangian L is equal to the kinetic energy of the system. Using Eqs. (3) – (5), one finally obtains to the following equation:

$$L(\dot\theta_0,\mathbf{q},\dot{\mathbf{q}}) = (1/2)\,D\,\dot\theta_0^2 + \dot\theta_0\,\mathbf{D}_{\mathbf{q}}\,\dot{\mathbf{q}} + (1/2)\,\dot{\mathbf{q}}^T\,\mathbf{D}_{\mathbf{qq}}\,\dot{\mathbf{q}} \tag{6}$$

where D, $\mathbf{D}_{\mathbf{q}}$, $\mathbf{D}_{\mathbf{qq}}$ are inertia-type matrices of appropriate dimensions which depend on configuration $\mathbf{q}$ and are given in Appendix A.

Note that L is a function of the spacecraft angular velocity $\dot\theta_0$ and of $\mathbf{q}$ and $\dot{\mathbf{q}}$ only, since the D-terms are functions of the configuration $\mathbf{q}$ and not of the spacecraft attitude θ_0. Then, the spacecraft attitude is an ignorable (cyclic) variable. The generalized momentum associated with this variable is:

$$b = \frac{\partial L}{\partial \dot\theta_0} = D\,\dot\theta_0 + \mathbf{D}_{\mathbf{q}}\,\dot{\mathbf{q}} = h_0 = const \tag{7}$$

In such case, one can construct a Routhian function $R(\mathbf{q},\dot{\mathbf{q}})$ of the system, given below [9]:

$$R(\mathbf{q},\,\dot{\mathbf{q}}) = L(\dot\theta_0,\mathbf{q},\dot{\mathbf{q}}) - b\,\dot\theta_0 \tag{7}$$

Substituting $\dot\theta_0$ by Eq. (1), as a function of $\mathbf{q}$ and $\dot{\mathbf{q}}$, the Routhian function takes the following form:

$$R(\mathbf{q},\dot{\mathbf{q}}) = \frac{1}{2}\,\dot{\mathbf{q}}^T\,\mathbf{H}(\mathbf{q})\,\dot{\mathbf{q}} + h_0\,D^{-1}\,\mathbf{D}_{\mathbf{q}}\,\dot{\mathbf{q}} - \frac{1}{2}\,h_0^2\,D^{-1} \tag{9}$$

where $\mathbf{H}(\mathbf{q})$ is an 2×2 positive definite symmetric matrix, called the reduced system inertia matrix, equal to [8],

$$\mathbf{H}(\mathbf{q}) = \mathbf{D}_{\mathbf{qq}} - \mathbf{D}_{\mathbf{q}}^T\,D^{-1}\mathbf{D}_{\mathbf{q}} \tag{10}$$

Note that the second term of $R(\mathbf{q},\,\dot{\mathbf{q}})$ is linear in the joint velocities and that the third term depends only on the configuration $\mathbf{q}$, hence, it acts like a potential. Applying Lagrange's equations on $R(\mathbf{q},\dot{\mathbf{q}})$, the following equations of motion result,

$$\boldsymbol{\tau} = \mathbf{H}(\mathbf{q})\,\ddot{\mathbf{q}} + \mathbf{C}_{\mathbf{h}}(h_0,\mathbf{q},\dot{\mathbf{q}})\,\dot{\mathbf{q}} + \mathbf{g}_{\mathbf{h}}(h_0,\mathbf{q}) \tag{11}$$

where $\boldsymbol{\tau}=\left[\tau_1,\tau_2\right]^T$ is the manipulator torque vector, with τ_i the torque applied to the i^{th} joint. The 2×2 matrix $\mathbf{C}_{\mathbf{h}}(h_0,\mathbf{q},\dot{\mathbf{q}})$ is a function of the system angular momentum and contains the nonlinear Coriolis and centrifugal terms:

$$\mathbf{C}_{\mathbf{h}}(h_0,\mathbf{q},\dot{\mathbf{q}}) = \mathbf{C}(\mathbf{q},\dot{\mathbf{q}}) + h_0\left[\frac{\partial}{\partial\mathbf{q}}\left\{D^{-1}\,\mathbf{D}_{\mathbf{q}}^T\right\} - \frac{\partial}{\partial\mathbf{q}}\left\{D^{-1}\mathbf{D}_{\mathbf{q}}\right\}\right] \tag{12}$$

where $\mathbf{C}(\mathbf{q},\dot{\mathbf{q}})$ is the matrix of nonlinear Coriolis and centrifugal terms when the initial angular momentum is zero, [8]. The vector $\mathbf{g}_{\mathbf{h}}(h_0,\mathbf{q})$ is also a function of the system angular momentum, given by Eq. (13):

$$\mathbf{g}_{\mathbf{h}}(h_0,\mathbf{q}) = \frac{1}{2}\,h_0^2\,\frac{\partial}{\partial\mathbf{q}}\left\{D^{-1}\right\} \tag{13}$$

The above methodology can be easily extended to a planar system consisting of a N dof manipulator.

Eqs. (12) – (13) show that for planar systems, $\mathbf{C}_{\mathbf{h}}$ and $\mathbf{g}_{\mathbf{h}}$ are independent of the spacecraft attitude and therefore the reduced dynamics are functions of $\ddot{\mathbf{q}}$, $\dot{\mathbf{q}}$ and $\mathbf{q}$ only.

III. Workspace And Speed Constraints

In this section, we study the existence of points in the

robot's reachable workspace where the end effector can remain indefinitely executing a task (e.g. satellite repair), in the presence of initial angular momentum. This is a quite demanding task, and in general it is an impossible one, when the angular momentum is non-zero. It is well known that in the absence of angular momentum, the end effector can remain at a point of the reachable workspace without the base being fixed. But the existence of angular momentum results to a system's motion according to the conservation of the angular momentum.

It is desired that the end effector location be fixed independently of the system's configuration. Having fixed end effector orientation in addition to a fixed location, is trivial, and can be addressed by adding a massless zero-length additional link. Therefore, we need to set,

$$(x_E, y_E) = const \tag{14}$$

Starting with Eq. (2), the solution to the inverse kinematic problem is given by:

$$q_1 = A\tan 2(s_{\theta_1}, c_{\theta_1}) - \theta_0 \tag{15a}$$

$$q_2 = A\tan 2(s_2, c_2) \tag{15b}$$

where,

$$c_2 = \frac{(x_E - \alpha c_{\theta_0})^2 + (y_E - \alpha s_{\theta_0})^2 - \beta^2 - \gamma^2}{2\beta\gamma} \tag{16a}$$

$$s_2 = \pm\sqrt{1 - c_2^2} \tag{16b}$$

$$c_{\theta_1} = \frac{(\beta + \gamma c_2)(x_E - \alpha c_{\theta_0}) + \gamma s_2 (y_E - \alpha s_{\theta_0})}{\beta^2 + \gamma^2 + 2\beta\gamma c_2} \tag{17a}$$

$$s_{\theta_1} = \frac{(\beta + \gamma c_2)(y_E - \alpha s_{\theta_0}) - \gamma s_2 (x_E - \alpha c_{\theta_0})}{\beta^2 + \gamma^2 + 2\beta\gamma c_2} \tag{17b}$$

where $c_2 = \cos q_2$ and $s_2 = \sin q_2$. In Eq. (16b), the + corresponds to the elbow-down manipulator configuration, while the – corresponds to the elbow-up one.

The inverse problem has a solution only if $-1 \le c_2 \le 1$, or

$$(\beta - \gamma)^2 \le r \le (\beta + \gamma)^2 \tag{18}$$

where

$$r = x_E^2 + y_E^2 + \alpha^2 - 2\alpha(x_E c_{\theta_0} + y_E s_{\theta_0}) \tag{19}$$

Note that the function $x_E c_{\theta_0} + y_E s_{\theta_0}$ can be written as:

$$x_E c_{\theta_0} + y_E s_{\theta_0} = \begin{bmatrix} x_E & y_E \end{bmatrix} \begin{bmatrix} c_{\theta_0} \\ s_{\theta_0} \end{bmatrix} = \sqrt{x_E^2 + y_E^2}\, c_\varphi = r_E c_\varphi \tag{20}$$

where φ is the angle between the two vectors appearing in Eq. (20), $c_\varphi = \cos\varphi$, and r_E is the distance between end effector and the system CM.

The extremes of r are:

$$r_{\min} = r_E^2 + \alpha^2 - 2\alpha r_E = (r_E - \alpha)^2, \quad \varphi = 0 \tag{21a}$$

$$r_{\max} = r_E^2 + \alpha^2 + 2\alpha r_E = (r_E + \alpha)^2, \quad \varphi = \pi \tag{21b}$$

Inequality (18) is satisfied only when

$$r_{\min} \ge (\beta - \gamma)^2, \; r_{\max} \le (\beta + \gamma)^2 \tag{22}$$

Inequalities (22) yield two solutions. The first one is:

$$\alpha + |\beta - \gamma| \le r_E \le \beta + \gamma - \alpha \tag{23a}$$

with $\alpha < \min(\beta, \gamma)$.

The second solution is:

$$r_E \le min(\alpha - |\beta - \gamma|, \beta + \gamma - \alpha) \tag{23b}$$

with $|\beta - \gamma| < \alpha < \beta + \gamma$. Equations (23) indicate bounds for the end-effector location that satisfy (14) and stem from kinematic requirements.

The above kinematic analysis is necessary but not sufficient. In addition, one must check that the dynamics constraint, i.e. the conservation of angular momentum is also satisfied.

The angular momentum conservation must be satisfied in conjunction with Eq. (14). Eq. (14) is equivalent to zero end effector linear velocity. The end effector linear velocity components can be obtained by differentiating Eqs. (2) with respect to time. Setting this velocity equal to zero, and writing it in matrix form along with Eq. (1), results in the following matrix equation,

$$\mathbf{A}(\theta_0, q_1, q_2) \begin{bmatrix} \dot\theta_0 & \dot\theta_1 & \dot\theta_2 \end{bmatrix}^T = \begin{bmatrix} h_0 & 0 & 0 \end{bmatrix}^T \tag{24}$$

where the zeros represent the zero linear velocity of end effector (i.e. $\dot x_E = 0,\ \dot y_E = 0$) and

$$\mathbf{A}(\theta_0, q_1, q_2) = \begin{bmatrix} D_0 & D_1 & D_2 \\ \alpha c_{\theta_0} & \beta c_{\theta_1} & \gamma c_{\theta_2} \\ \alpha s_{\theta_0} & \beta s_{\theta_1} & \gamma s_{\theta_2} \end{bmatrix} \tag{25}$$

Assuming that matrix $\mathbf{A}$ is not singular, Eq. (24) yields,

$$\dot\theta_0 = \frac{\beta\gamma s_2}{S(q_1, q_2)} h_0 \tag{26a}$$

$$\dot q_1 = -\frac{\alpha\gamma s_{12} + \beta\gamma s_2}{S(q_1, q_2)} h_0 \tag{26b}$$

$$\dot q_2 = \frac{\alpha\beta s_1 + \alpha\gamma s_{12}}{S(q_1, q_2)} h_0 \tag{26c}$$

where $s_1 = \sin q_1$, $s_{12} = \sin(q_1 + q_2)$ and

$$S(q_1, q_2) = \det(\mathbf{A}) = \alpha\beta D_2 s_1 + \beta\gamma D_0 s_2 - \alpha\gamma D_1 s_{12} \tag{27}$$

Eqs. (26b)-(26c) allow one to plan joint motions so that the end effector remains fixed. The spacecraft angular velocity that will result is given by Eq. (26a).

Note that the configuration rates in Eqs. (26) are proportional to the initial angular momentum and vanish when the momentum is zero, i.e. the system can always remain at fixed location without executing any motions when its angular momentum is zero.

When $\mathbf{A}$ is singular (i.e. $S(q_1, q_2) = 0$), the configuration rates, given by Eqs. (26), increase to infinity and the end effector is displaced from its desired location. Equation $S(q_1, q_2) = 0$ corresponds to a joint space surface. If this surface is mapped to the Cartesian space, then it defines circles with radii that depend on system parameters and define an area where the dynamics constraints are satisfied. Satisfaction of both the kinematics and dynamics constraints, yields the workspace part at which the end effector can remain indefinitely, despite the accumulated momentum.

IV. Application Example

To illustrate the methodology described above, a free-floating space manipulator with the structure shown in Fig. 1 is employed. The system parameters are given in Table I.

TABLE I
SYSTEM PARAMETERS

Body	$l_i(m)$	$r_i(m)$	$m_i(Kg)$	$I_i(Kg\cdot m^2)$
0	0.5	0.5	400	66.67
1	1.0	1.0	40	3.33
2	0.5	0.5	30	2.50

The grey area in Fig. 2 represents the workspace area where kinematics and dynamics constraints are satisfied. Fig. 2 also shows snapshots of the motion of the free-floating space manipulator system for a desired end effector fixed position at $x_E = 1.5\,m$, $y_E = 1m$. This point, according to Eq. (23a), is a feasible one and belongs to the grey area. The base initial orientation is $\theta_0(0) = 0^o$ and the initial angular momentum of the system is $h_0 = 0.5\,Nms$. The duration of motion is chosen to be $t_f = 2000\,s$, but could be arbitrary long. The system configuration is given by Eqs. (15), which yield $[q_1(0),\ q_2(0)] = [76^o, -125^o]$. The initial configuration rate is given by Eqs. (26). For the above angular momentum, the initial angle rates are found to be $[\dot{\theta}_0(0),\ \dot{q}_1(0),\ \dot{q}_2(0)] = [7.5, -9.1, -2.2]*10^{-3}\,rad/s$. It can be seen that while the end effector remains at a fixed location, the base of the system rotates slowly and the manipulator executes an oscillatory motion in such a way so as to have the system's angular momentum conserved.

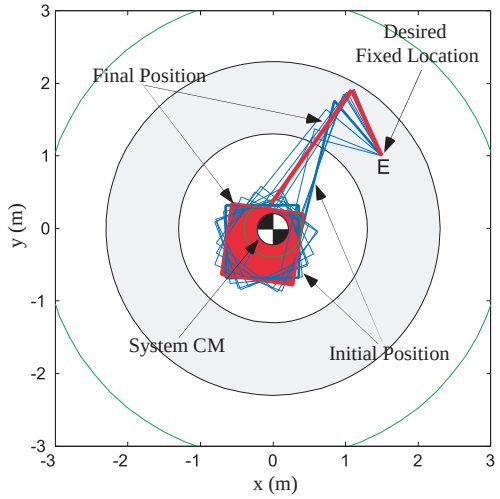

Fig. 2. Motion animation of space manipulator with $h_0 = 0.5\,Nms$.

The trajectories and the rates of the configuration variables are shown in Fig. 3(a), (b). It can be seen that all trajectories are smooth throughout the motion. The first joint angle increases with time, therefore a special joint design must be employed. The joint torques that correspond to the motion in Fig. 2 are computed using Eq. (11) and are displayed in Fig. 3(c). The required torques are small and smooth, guaranteeing motion feasibility. Note that the configuration rates are proportional to the system angular momentum, see Eqs. (26). Therefore, if the initial momentum is doubled (i.e. $h_0 = 1\,Nms$), these rates will double, and the system will execute the same motion as before, but in the half time, as can be shown in Fig. 4(a), (b). However, the required joint torques, given by Eq.(11) will be larger, since the increase is not proportional to the increase in the angular momentum, see Fig. 4(c). This is due to the fact that the $\mathbf{C}_h$ terms are nonlinear functions of the joint rates.

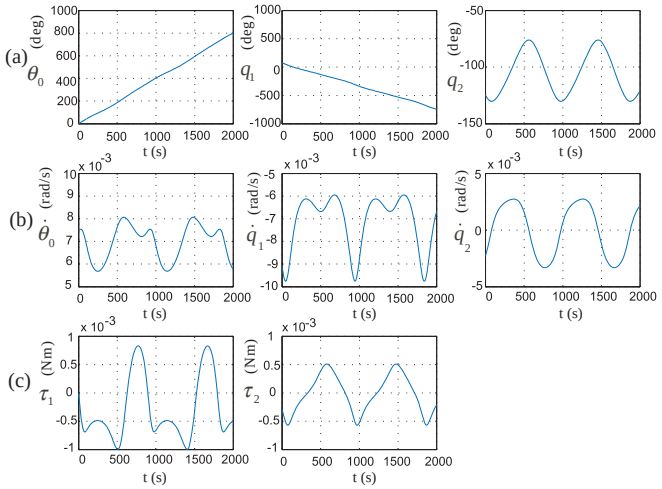

Fig. 3. $h_0 = 0.5\,Nms$: (a) Trajectories of spacecraft attitude and relative joint angles, (b) rates of spacecraft attitude and relative joint angles and (c) torques on manipulator forearm and upper arm.

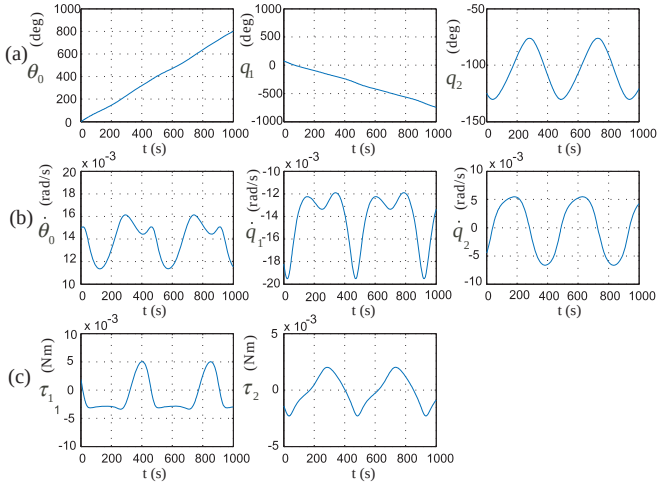

Fig. 4. $h_0 = 1\,Nms$: (a) Trajectories of spacecraft attitude and relative joint angles, (b) rates of spacecraft attitude and relative joint angles and (c) torques on manipulator forearm and upper arm.

V. Hardware Space Robot Emulator

At the NTUA, an experimental testbed was developed for motion studies in zero gravity. The hardware planar emulator consists of a granite table of negligible roughness, and a small robot supported by three airbearings, see Fig. 5(a). The robot is capable of horizontal frictionless motion on the table, thus allowing for 2D emulation zero gravity in a laboratory environment. The robot is fully autonomous. Its propulsion autonomy is achieved by an on-board CO_2 tank used to provide gas to the air bearings and to three couples

of propulsion thrusters. The robot is also equipped with a reaction wheel to control the robot's angular momentum. The computational autonomy is achieved with a PC104 mounted on the robot. Power autonomy is achieved with a set of on-board batteries. The novelty of this configuration is that the robot is not only of low mass and completely self-contained but also it is composed of subsystems similar to those of a space system, therefore making the emulator significantly more realistic. The simulator provides a low-cost, long duration, and easily reconfigurable platform that allows for the experimental validation of different control, dynamics, and planning schemes, facilitating the transition from analysis to application. Next, we describe the main characteristics of the emulator.

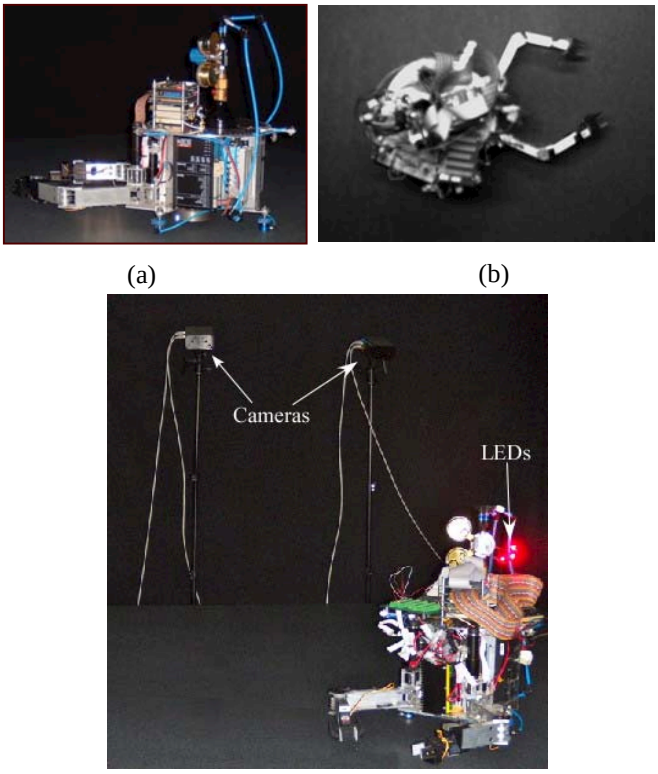

Fig. 5. (a) The robot floating over the granite table, (b) an image from the overhead camera, (c) robot and motion tracking cameras.

A. Sensors

Three different systems for measuring the position and orientation are used. Two of those will be permanently employed.

(a) *Camera*: An overhead camera is located above the field of action of the robot for finding its position and orientation. To this end, three LEDs are mounted at the corners of a triangle, on top of the robot, and are tracked by the camera. Its images, see Fig. 5(b), are transmitted to an off-board computer, where a real-time image processing process determines robot position and orientation. This information is sent wirelessly via TCP/IP to the space robot's processing unit.

(b) *Optical Sensors*: The sensors are mounted next to the airbearings and employ optical flow techniques; by comparing successive photos of the granite surface, they measure the differential displacement at each sampling instant versus the position at the previous instant, and provide a local pair of displacements dx and dy. Two sensors with known distance among them, produce therefore four values per instant, and the three unknown parameters (x, y, and θ) can be calculated geometrically. Optical sensors have the advantages of having a very high sampling rate, compact size, excellent accuracy and low cost. Their main disadvantage is that the accumulation of error and sudden reading jumps. Therefore, this system is used in conjunction to the overhead camera, allowing for periodic resetting of the coordinates.

(c) *Motion Tracking System*: The system consists of six high speed PhaseSpace cameras placed around the granite table, Fig. 5(c), one LED base station, two LED driver units and thirty active LED Markers mounted on the robot. Each LED emits in its own frequency, controlled by the base station and driver unit. The cameras recognize the position of each LED and send it to an off-board server, which determines the robot position and orientation in real-time and at a 1 mm accuracy. The system has the advantages of great accuracy and resolution independently of light conditions and sufficient capture space. Its main disadvantage is the high cost. It is used here to validate the accuracy of the previous two systems.

(d) *Other Sensors*: A number of other sensors are used also. These include force, Hall, and voltage sensors and encoders. Force sensors are used to measure gripper-applied forces. Hall sensors on the manipulators, signal to the PC104 the reach of the maximum joint angles. Voltage meters, and other proprioceptive sensors on the motherboard inform the user, a PIC microcontroller, and the PC104 of possible malfunctions, in order for emergency actions to be performed. Additionally, each motor is equipped with digital encoders that send joint angular positions to the PC104.

B. Actuators

(a) *Thrusters*: Propulsion is achieved by six CO_2 thrusters, and a number of regulators that reduce the CO_2 tank pressure to 7 bar. The electronic circuitry actuates 2-way on-off solenoid valves to control the thruster gas flow using Pulse Width Modulation (PWM), see Fig. 6(a). The use of PWM allows the development of thrust in a continuous range, using the on-off thruster technology, which is common in actual space applications.

(b) *Reaction Wheel*: To reduce gas consumption, a reaction wheel providing torque around a vertical axis was designed and installed, see Fig. 6(b). The wheel was chosen due to the simple control algorithm, attitude fine-tuning capability, and best fit to the two-dimensional experiment. The wheel is actuated by a torque-controlled DC servomotor.

(c) *Robotic Arms*: The robot has two two-dof manipulators, see Fig. 5(a), actuated by DC motors and commanded by the PC104. They have integrated gears for high torque output and are all installed on the main robot chassis. A sophisticated transmission design employing inextensible micro wires and pulleys enables the

independent motion of each link. Each manipulator is equipped with a DC servomotor-actuated and force sensing gripper for capturing of other objects. These grippers can be removed easily and so as to attach an alternative type of gripper or tool.

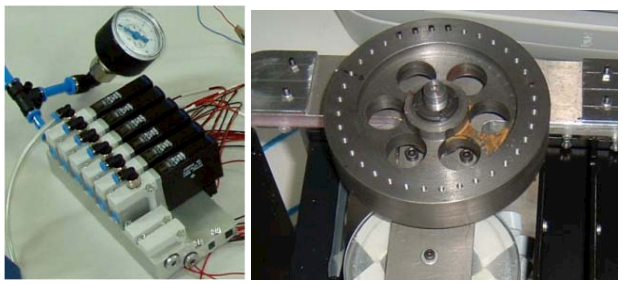

(a) (b)

Fig. 6. (a) Thruster solenoid valves, (b) the reaction wheel.

C. PC104 and RTOS

An on-board PC104 computer, chosen for its high efficiency, robustness and low power requirements, is used for computational autonomy. The PC104 includes a CPU module (Intel Celeron 648MHz, 495MB RAM), two incremental encoder card modules, an analog output module, a wireless LAN module and a hard disk module. Each encoder card module is capable of handling up to three incremental 16-bit encoder inputs, has three 16-bit timers and 24 digital I/O lines.

The analog output module has eight 12-bit analog output channels and 24 digital I/O lines. The CPU module includes a real time clock and all primary I/O functions (USB, parallel port, serial port, etc.). The PC104 is responsible for motor and thruster control, and reads sensors such as the optical sensors (via the USB port), and the overhead camera (via wireless Ethernet). The PC104 is running under a dual boot of Arch Linux 2.4.29 RTL and QNX 6.3.0; both operating systems have real time capabilities and the programming language of choice is C.

Currently, this emulator is being used to experimentally verify the simulation results that were presented here.

CONCLUSIONS

In this paper, we studied the influence of initial angular momentum on the behavior of a free-floating space robot. We focused on the determination of locations of the robot's reachable workspace where its end effector can remain executing a task (e.g. a satellite repair) indefinitely. The proposed method used the kinematics and dynamics constraints, which arise from system's dynamics and allow the computation of such locations for various systems. The method was illustrated by an example. A successful deployment requires experimental task validation. With this aim, we presented the main characteristics of the hardware space robot simulator developed at the NTUA. The simulator is being used to verify experimentally the concept here.

REFERENCES

[1] Yoshida, K., Hashizume, K., and Abiko, S., "Zero Reaction Maneuver: Validation with ETS-VII Space Robot and Extension to Kinematically Redundant Arm," *Proc. IEEE International Conference on Robotics and Automation (ICRA '01)*, Seoul, Korea, May 2001, pp. 441-446.

[2] Rekleitis, I., Martin, E., Rouleau, G., L'Archeveque, R., Parsa, K., and Depuis, E., "Autonomous Capture of a Tumbling Satellite," *In Journal of Field Robotics, Special Issue on Space Robotics, 24(4)*, 2007, pp. 275-296.

[3] Matsuno, F. and Saito, K., "Attitude Control of a Space Robot with Initial Angular Momentum," *Proc. IEEE International Conference on Robotics and Automation (ICRA '01)*, Seoul, Korea, May 2001, pp. 1400-1405.

[4] Wertz, J, Chen. A, et al., "SPHERES: A Testbed for Long Duration Satellite Formation Flying in Micro-Gravity Conditions", *Proc. of the AAS/ AIAA Space Flight Mechanics Meeting*, Clearwater, FL, January 23-26, 2000.

[5] Adams, J., Robertson A., Zimmerman K., How J., "Technologies for Spacecraft Formation Flying", *Proc. of the Institute of Navigation GPS-96 Conference*, pp. 1321-1330, Kansas City MO, September 1996.

[6] Bettanini, C., et. al., "Improving the Free-floater Space Robot Simulator for Intervention Missions", *Proc. of the 7th International Symposium on Artificial Intelligence, Robotics and Automation in Space (i-SAIRAS 2003)*, NARA, Japan, May 19-23, 2003.

[7] Nakamura, Y., Sasaki F. and Nakasuka, S., "Guidance and Control of Tethered Retriever with Collaborative Tension-Thruster Control for Future On-Orbit Service Missions", *Proc. of the 8th International Symposium on Artificial Intelligence, Robotics and Automation in Space (i-SAIRAS 2005)*, Munich, Germany, Sept. 5-8, 2005.

[8] Papadopoulos, E., "Nonholonomic Behavior in Free-floating Space Manipulators and its Utilization," *Chapter in Nonhonomic Motion Planning, Zexiang Li and J. F. Canny, Eds.*, Boston: Kluwer Academic 1993, pp. 423-445.

[9] Goldstein, H., Poole, C., and Safko, J., "Classical Mechanics," *3rd Edition, Addison Wesley*, 2002.

APPENDIX A

The *D*-terms are given below:

$$D_j = \sum_{i=0}^{2} d_{ij} \quad (j = 0,1,2) \tag{A1}$$

$$D = D_0 + D_1 + D_2 \tag{A2}$$

$$\mathbf{D_q} = \begin{bmatrix} D_1 + D_2 & D_2 \end{bmatrix} \tag{A3}$$

$$\mathbf{D_{qq}} = \begin{bmatrix} d_{11} + 2\,d_{12} + d_{22} & d_{12} + d_{22} \\ d_{12} + d_{22} & d_{22} \end{bmatrix} \tag{A4}$$

$$d_{00} = I_0 + m_0\,(m_1 + m_2)\,r_0^2 / M \tag{A5}$$

$$d_{10} = m_0\,r_0\,(l_1\,(m_1 + m_2) + r_1\,m_2)\,c_1 / M = d_{01} \tag{A6}$$

$$d_{20} = m_0\,m_2\,r_0\,l_2\,c_{12} / M = d_{02} \tag{A7}$$

$$d_{11} = I_1 + (m_0\,m_1\,l_1^2 + m_1\,m_2\,r_1^2 + m_0\,m_2\,(l_1 + r_1)^2) / M \tag{A8}$$

$$d_{21} = m_2\,l_2\,(m_1\,r_1 + m_0\,(l_1 + r_1)\,c_2) / M = d_{12} \tag{A9}$$

$$d_{22} = I_2 + m_2\,(m_0 + m_1)\,l_2^2 / M \tag{A10}$$

$$M = m_0 + m_1 + m_2 \tag{A11}$$

where $c_1 = \cos q_1$, $c_{12} = \cos(q_1 + q_2)$.

The α, β, γ terms are given by:

$$\alpha = m_0\,r_0 / M \tag{A12}$$

$$\beta = (m_0\,l_1 + r_1\,(m_0 + m_1)) / M \tag{A13}$$

$$\gamma = r_2 + (m_0 + m_1)\,l_2 / M \tag{A14}$$